

## Article

# Synergistic Electrochemical Properties of Graphene Incorporated LCZ-Oxide Cathode for Low Temperature Solid Oxide Fuel Cell

Muhammad Ashfaq Ahmad <sup>1,2</sup>, Khalil Ahmad <sup>3</sup>, Hu Li <sup>1,4,\*</sup> , Abdelaziz Gassoumi <sup>5,6</sup>, Rizwan Raza <sup>1,2</sup> , Muhammad Saleem <sup>7</sup>, Syed Hassan Mujtaba Jafri <sup>8</sup>  and Ghazanfar Abbas <sup>2,\*</sup> 

<sup>1</sup> Shandong Technology Centre of Nanodevices and Integration, School of Microelectronics, Shandong University, Jinan 250101, China

<sup>2</sup> Clean Energy Research Lab (CERL), Department of Physics, COMSATS University Islamabad, Lahore Campus, Lahore 54000, Pakistan

<sup>3</sup> Departments of Physics, Virtual University of Pakistan, Lahore 54000, Pakistan

<sup>4</sup> Shenzhen Research Institute, Shandong University, Shenzhen 518057, China

<sup>5</sup> Department of Physics, Faculty of Science, King Khalid University, P.O. Box 9004, Abha 61413, Saudi Arabia

<sup>6</sup> Laboratoire de Physique de la Matière Condensée LPMC, Département de Physique, Faculté des Sciences de Tunis, Université Tunis El Manar, Tunis 2092, Tunisia

<sup>7</sup> Institute of Physics, The Islamia University of Bahawalpur, Bahawalpur 63100, Pakistan

<sup>8</sup> Department of Electrical Engineering, Mirpur University of Science and Technology (MUST), Mirpur 10250, Pakistan

\* Correspondence: hu.li@sdu.edu.cn (H.L.); mian\_ghazanfar@hotmail.com (G.A.)

**Abstract:** Mixed metallic oxides are getting increasing attention as novel electrode materials for energy conversion devices. However, low mixed ionic-electronic conductivity and high operating temperature hamper the practical applications of these devices. This study reports an effective strategy to improve the conductivity and performance of the fuel cell at low temperature by partially incorporating graphene in the  $\text{Li}_{0.1}\text{Cu}_{0.2}\text{Zn}_{0.7}$ -oxide (LCZ) composite. The proposed cathode material is synthesized via the cost effective conventional solid-state route. Graphene incorporated LCZ shows excellent performance, which is attributed to the favorable charge transport paths offering low area-specific resistance. An X-ray diffractometer (XRD) and scanning electron microscope (SEM) are employed for microstructural and surface morphological analyses, respectively. Electrical conductivities of all the materials are determined by the DC four probe method, and interestingly, LCZ-1.5% graphene exhibits an excellent conductivity of 3.5 S/cm in air atmosphere at a temperature of 450 °C with a minimum value of 0.057  $\Omega\text{cm}^2$  area-specific resistance (ASR) that demonstrates significantly good performance. Moreover, the three-layer fuel cell device is fabricated using sodium carbonated  $\text{Sm}_{0.2}\text{Ce}_{0.8}\text{O}$  (NSDC) as an electrolyte, which can operate at low temperatures exhibiting open circuit voltage 0.95 V and shows a peak power density, i.e., 267.5  $\text{mW}/\text{cm}^2$  with hydrogen as the fuel.

**Keywords:** nanocomposite; cathode materials; LTSOFC; graphene incorporation; power density



**Citation:** Ahmad, M.A.; Ahmad, K.; Li, H.; Gassoumi, A.; Raza, R.; Saleem, M.; Jafri, S.H.M.; Abbas, G. Synergistic Electrochemical Properties of Graphene Incorporated LCZ-Oxide Cathode for Low Temperature Solid Oxide Fuel Cell. *Crystals* **2023**, *13*, 434. <https://doi.org/10.3390/cryst13030434>

Academic Editors: Fengyu Shen and Yucun Zhou

Received: 20 January 2023

Revised: 26 February 2023

Accepted: 27 February 2023

Published: 2 March 2023



**Copyright:** © 2023 by the authors. Licensee MDPI, Basel, Switzerland. This article is an open access article distributed under the terms and conditions of the Creative Commons Attribution (CC BY) license (<https://creativecommons.org/licenses/by/4.0/>).

## 1. Introduction

The increasing population and industrialization in contemporary times have increased energy consumption in the modern world. Conventional fossil fuels are unable to meet the unprecedented demand of energy resources. This scarcity of conventional resources, along with their hazards of environment pollution, stimulate researchers to discover, invent, explore, and improve renewable, clean, and sustainable energy resources [1,2]. Consequently, developing sustainable, environment-friendly, and high-efficiency energy assets is one of the most challenging tasks these days. Several energy conversion devices such as batteries, super capacitor fuel cells, and solar cells based on renewable energy

resources such as hydrogen fuel and solar energy have already demonstrated their efficiency, but they come with limited practical applications [3]. Fuel cells offer electrical energy by converting chemical energy with high efficiency and zero emission and is categorized into various types, depending upon the electrolyte materials being utilized [4].

Solid oxide fuel cell gained attention due to its higher efficiency, low emission, and fuel flexibility as compared to the other fuel cell families [5–7]. At the same time, solid oxide fuel cells (SOFC) have certain limitations, such as high operating temperatures (800–1000 °C), precious electrode materials, and degradation of the material, which hamper their production at the commercial level [8]. Lowering the operating temperature and developing electrodes material with good electrical and catalytic behavior have been the ambitions of the fuel cell community [9]. Composite materials based on nickel yttrium-stabilized zirconia (Ni-YSZ) are widely used electrodes for conventional SOFC with YSZ as the electrolyte exhibiting good catalytic and electrical properties at 1000 °C. The same electrode materials can work at 800 °C with gadolinium-doped ceria (GDC) and samarium-doped ceria (SDC) without sacrificing the results [10]. However, the current temperature is still high and remains a major challenge to commercialize SOFC technology, including the carbon deposition, poisoning on the layer, and poor oxidation for hydrocarbon fuel issues [11].

Lowering the operational temperature for SOFC and decreasing the polarization resistance of the cathode is a big dream of the fuel cell research community [12]. A major contribution of polarization losses has been observed usually at the cathode layer [13]. Lanthanum strontium iron  $\text{La}_{0.8}\text{Sr}_{0.2}\text{FeO}_3$  (LSF), lanthanum strontium manganese  $\text{La}_{0.8}\text{Sr}_{0.2}\text{MnO}_3$  (LSM), and samarium strontium cobalt  $\text{Sm}_{0.5}\text{Sr}_{0.5}\text{CoO}_{3-\delta}$  (SSC) are widely used as the cathode materials. LSM is being developed due to its stable attribution with yttrium-stabilized zirconia (YSZ) at higher temperatures [14]. Huang et al. reported a LSFN inspection as a cathode exhibiting improved electrical conductivity and ionic conduction beyond 550 °C [15].  $\text{Ba}_x\text{Sr}_{1-x}\text{FeO}_{3-\delta}$ ,  $\text{La}_{0.8}\text{Sr}_{0.2}\text{FeO}_{3-\delta}$  perovskite oxide cathode materials are based on, are commonly proposed in terms of electrical conductivity and thermal stability for intermediate-temperature IT-SOFC [16].

Improved performances have been obtained by the nanostructure approach [17,18] and composite electrodes of transition metal oxides such as NiO, CuO,  $\text{Fe}_2\text{O}_3$ , SrO, and ZnO [19,20]. Nanocomposite-based cathode materials LSMZ developed with SDC were found compatible for low-temperature solid oxide fuel cells [21]. A ZnO-modified lithiated NiO composite cathode has been reported as a good material for electrocatalytic oxygen reduction activity with a yielded power density of 808 mW/cm<sup>2</sup> and polarization resistance of 0.22 Ωcm<sup>2</sup> at 550 °C [22]. A zinc-based nanostructured  $\text{Mn}_{0.20}\text{Fe}_x\text{Zn}_{0.80-x}\text{O}_\delta$  composite has been examined as a suitable electrode using natural gas fuel over a temperature of 600 °C [23].

Graphene, a monolayer of carbon atoms, exhibits ultra-high porosity, large specific area, and good electronic and electrochemical properties [24], has shown excellent catalytic performance for LT-SOFC [25] and the YSZ/rGo composite displayed good electrochemical applications in the temperature range 150–800 °C [26]. Graphene with groups 4–9 has been reported as electrocatalysts in oxygen evolution reactions (OER) and oxygen reduction reactions (ORR) [27]. Composites of other nanomaterials such as sulfides, metal–metal oxides, alloys, and polymeric materials exhibited interactive effects with graphene and found it a potential candidate for energy conversion and storage devices [28–30].

The present work focuses on incorporating graphene into LCZ oxide with different weight ratios to study its applications as a cathode material for LT-SOFC. The effects of Gr on electrical conductivity and catalytic activity are examined and found very synergistic. A significant enhancement of the fuel cell performance is also observed by fabricating a three-layers fuel cell device at low temperatures in a hydrogen atmosphere.

## 2. Experimental Technique

### 2.1. Synthesis of Cathode Materials

The cathode was prepared by the conventional solid-state reaction method. The stoichiometric molar ratio of composition  $\text{Li}_{0.1}\text{Cu}_{0.2}\text{Zn}_{0.7}$  oxide using  $\text{Li}_2\text{CO}_3$ ,  $\text{CuCO}_3\cdot\text{Cu}(\text{OH})_2$ , and  $\text{ZnO}$  (all from Sigma Aldrich, St. Louis, MO, USA) were used as starting materials. The planned precursor powders were mixed in mortar and ground with pestle to make a homogeneity of the mixture. This mixture was sintered at  $800\text{ }^\circ\text{C}$  in a furnace for 4 h. The sintered powder was again ground for 25 min, and a fine homogenous composite powder of LCZ material was obtained. The as-prepared graphene via cost effective and eco-friendly electrolysis method [31] was used to incorporate into the LCZ composite. Three samples were prepared and assigned named as 0 wt.% Gr-LCZ (pure), 1 wt.% Gr-LCZ, and 1.5 wt.% Gr-LCZ.

### 2.2. Characterizations

The XRD pattern of all sintered samples was analyzed by PAN-Alytical X'Pert Pro with  $\text{Cu K}\alpha$  radiation, ( $\lambda = 1.5418\text{ \AA}$ ), 40 kV voltage, and 30 mA currents at room temperature. The surface morphology and homogeneity of the prepared composites was analyzed by SEM (TESCAN Vega 3 LMU). The FTIR analysis of prepared LCZ and graphene incorporated LCZ cathode materials was carried out to examine the structure and phase transformation information by using FTIR spectrophotometer at a consistent spectral resolution of  $6\text{ cm}^{-1}$  in the range of  $4000\text{--}500\text{ cm}^{-1}$  by taking 116 scans.

### 2.3. Conductivity Measurements

The electrical conductivities of proposed synthesized LCZ-pure, 1 wt.% Gr-LCZ, and 1.5 wt.% Gr-LCZ cathode materials were measured using four-probe DC method with 2450 SMU (Keithley instrument, Taiwan) from  $300\text{ to }600\text{ }^\circ\text{C}$  range in the air atmosphere. For this purpose, pellets (13 mm diameter and 2 mm thickness) of each sample were prepared by hydraulic press using  $280\text{ kg/cm}^2$ , followed by sintering at  $550\text{ }^\circ\text{C}$  for 45 min. Silver paste was painted on the both sides of the pellets for conductivity measurements. The area-specific resistance of all the materials was calculated from conductivity data and was plotted as a function of temperature in the range of  $300\text{--}600\text{ }^\circ\text{C}$ .

### 2.4. Fuel Cell Fabrication and Performance

In order to fabricate three-layer fuel cells, the already prepared 20 wt.% ratio of NSDC electrolyte was added in LCZ and graphene-incorporated LCZ cathode materials to make suitable composite for electronic and ionic conductive phenomenon. It was then co-pressed using conventionally prepared LNCZ as the anode and NSDC as the electrolyte [32] under a pressure of  $280\text{ kgcm}^{-2}$ . Fuel cell pellets of 13 mm diameter and 1 mm thickness were painted by silver paste on outer surfaces to collect current. However, the active area was considered  $0.64\text{ cm}^2$  on behalf of the dimension of sample holder. Fuel cell performance was executed by using fuel cell testing unit (S102, China) fed by hydrogen as fuel (flow rate  $110\text{ mL min}^{-1}$ ) at anode and air as oxidant (flow rate  $80\text{ mL min}^{-1}$ ) at cathode side. I-V and I-P curves were drawn from data recorded at  $600\text{ }^\circ\text{C}$ .

The scheme of fabrication of three-layers cell has been prescribed as below:

LCNZ as anode (already prepared), NSDC (already prepared) as the cathode and LCZ-pure and LCZ-graphene as the cathode (synthesized in this work).

(80 wt.% LCNZ-20 wt.% NSDC/NSDC/80 wt.% LCZ-pure-20 wt.% NSDC and 80 wt.% LCNZ-20 wt.% NSDC/NSDC/80 wt.% LCZ-graphene-20wt.%).

The dimensions are as LCNZ-NSDC Anode layer 45 mg, NSDC Electrolyte layer 25 gm, and LCZ-pure-NSDC 25 mg for cell 1.

The dimensions are the LCNZ-NSDC Anode layer: 45 mg, NSDC Electrolyte layer: 25 gm, and LCZ-graphene-NSDC: 25 mg for cells 2 and 3.

### 3. Results and Discussion

The LCZ oxide includes the starting materials  $\text{Li}_2\text{CO}_3$ ,  $\text{CuCO}_3 \cdot \text{Cu}(\text{OH})_2$ , and  $\text{ZnO}$  is a composite material. Figure 1 shows the X-ray diffraction patterns of LCZ-pure and LCZ-Gr composites sintered at  $800^\circ\text{C}$  for four hours. The XRD analysis depicted the two phase materials ZnO and CuO. As earlier, Zhang et al. 2014 developed strontium and magnesium doped gallate LSGM oxide electrolyte for SOFC and found two phases,  $\text{LaSrGaO}_4$  and  $\text{LaGaO}_3$  in XRD data [33]. The indexing of all the peaks of ZnO phase illuminated the hexagonal structure confirmed with JCPDs card No. 089-0511 having space group  $p63mc$ . The lattice constants were calculated and found to be  $a = b = 3.24$  and  $c = 5.20 \text{ \AA}$ . The diffracted peaks for ZnO were detected at  $31.77^\circ$ ,  $34.43^\circ$ ,  $36.26^\circ$ ,  $47.55^\circ$ ,  $56.14^\circ$ ,  $62.87^\circ$ ,  $66.39^\circ$ ,  $67.96^\circ$ ,  $69.10^\circ$ ,  $72.16^\circ$ , and  $76.98^\circ$  correspond to crystal plans (100), (002), (101), ( $\bar{1}02$ ), (110), (103), (200), (112), (201), (004) and (202), respectively. The second phase executed the monoclinic structure of tenorite CuO (space group  $C2/c$ ) with lattice constants  $a = 4.65$ ,  $b = 3.41$  and  $c = 5.10 \text{ \AA}$  according to JCPDs card No. 01-1117. The peaks at  $35.74^\circ$ ,  $38.95^\circ$ ,  $53.88^\circ$ ,  $61.8^\circ$  and  $66.22^\circ$  correspond to crystal plans ( $\bar{1}11$ ), (111), (020), ( $\bar{1}13$ ) and (022) of CuO, respectively. High crystalline structure of the prepared compositions was observed as revealed by the obtained sharp peaks. The two phases depict the composite behavior of the proposed material which contribute individually for better conductivity and electrochemical performance of fuel cell [34,35]. The two -phase structure, based on XRD results, offers co-existence involvement of ZnO and CuO in the composite. The XRD patterns did not detect obvious graphene peaks for LCZ-Gr samples due to its amorphous nature; however, graphene was incorporated in LCZ materials [36]. The crystallite sizes were calculated using the Scherrer's formula and were found to be in 80–115 nm range from strong and intense peaks.

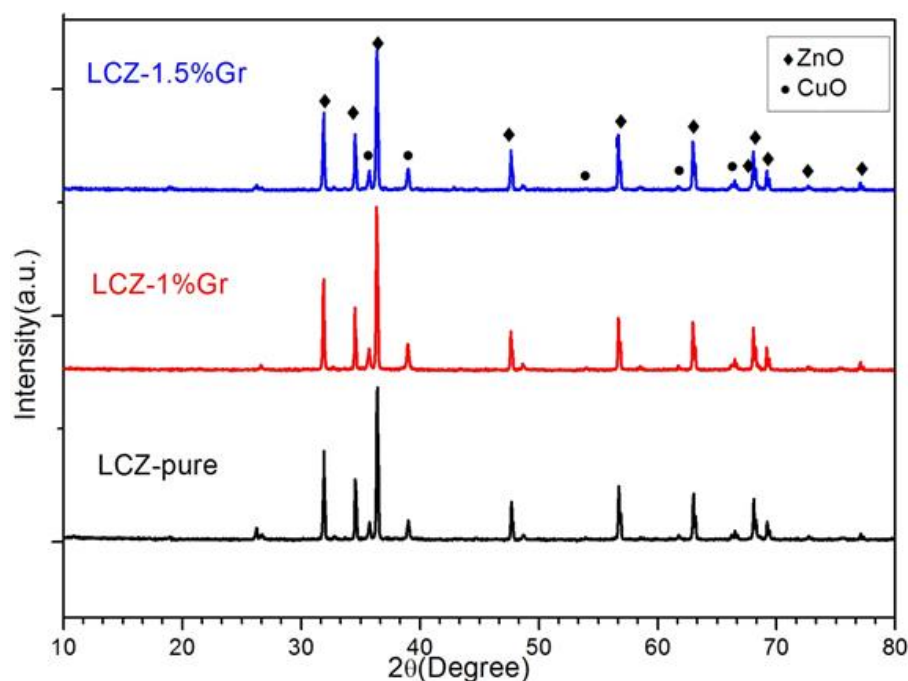


**Figure 1.** XRD pattern for LCZ-pure and graphene incorporated materials sintered at  $800^\circ\text{C}$  for four hours.

The surface morphology and microstructure of prepared samples were examined by SEM and are displayed in Figure 2a–c. Oval-shaped structure, along with distributed powder on these structures, was observed with compact densification in Figure 2c. Oval shaped morphology of composite material reflected the layers compaction of precursors sintered at high temperature. Smooth surface, along with pores, can be observed in the images displayed in Figure 2. Few small whitish-like particles on surface might attribute

the dispersion of graphene powder. However, the whitening loops over the particles were not observed in LCZ-pure image shown in Figure 2a. On investigating the surface morphology of SEM images by line drawing, the particle sizes were found to be in the range of 90–125 nm and validated the XRD findings. These expressions illustrate that the prepared material is homogenous and well porous. Such porous structure in cathode material provides more channels for the passage of electrons and oxygen ions during the conduction mechanism of cell reaction [37,38]. The energy dispersive X-ray (EDX) spectrum of base sample is displayed in Figure 3. The spectrum depicts the presence of transition metal elements of zinc (Zn) and copper (Cu). No obvious peak appeared for Li in EDX spectrum due to light weight element having minor stoichiometry amount in the composition. The conventional EDX instrument cannot detect elements lighter than boron. These special detectors have a limit of detection of about 20 wt.%. Due to its spread as whitish loops over LCZ in SEM images clarify the existence of Gr in LCZ material. However, in XRD for the structural analysis and EDX for the elemental analysis could not be detected due to its amorphous nature. For more evidence, Esmaeili et al. 2020 reported that meaningful picture of element distribution on the surface verified the presence of carbon, oxygen and iron elements throughout the surface of GO-PEG-Fe<sub>3</sub>O<sub>4</sub>. The reported EDX spectra further showed the corresponding peaks of carbon (C) oxygen (O) and iron (Fe) in the final conjugate [39].

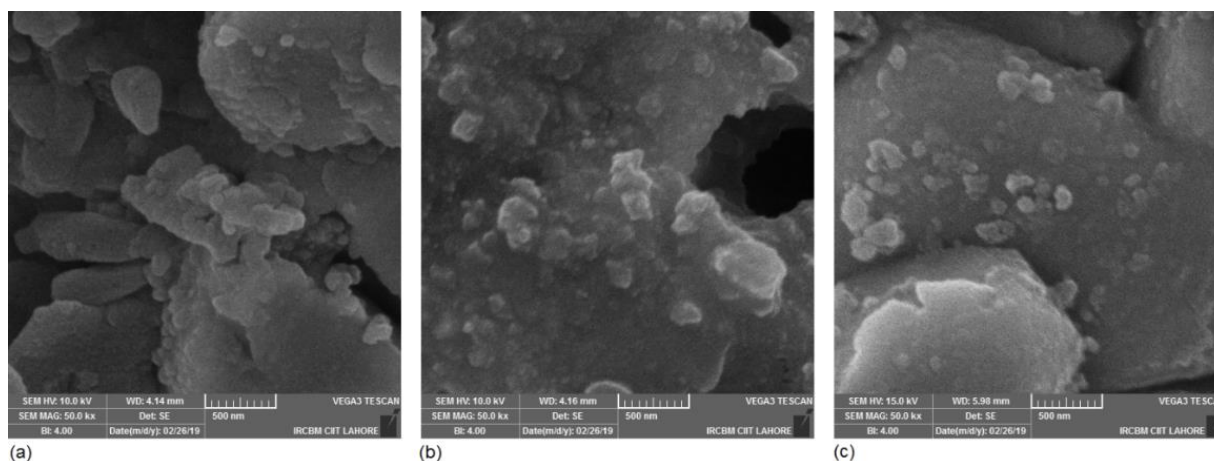


**Figure 2.** Scanning electron microscopy (SEM) images (a) LCZ-pure; (b) 1 wt.% Gr-LCZ; (c) 1.5 wt.% Gr-LCZ.

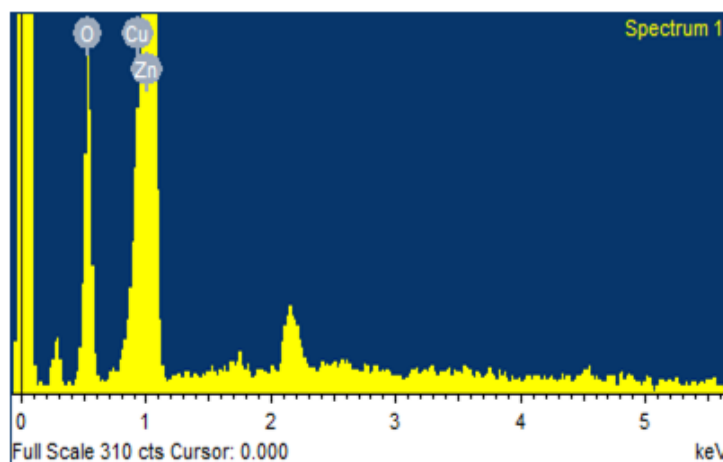


**Figure 3.** EDX spectra of the LCZ sample.

The FTIR spectrum of the prepared composite material is shown in Figure 4. The information regarding the prepared materials structural and phase transformation phenomenon

was studied by FTIR spectroscopy in wavelength of 4000–500  $\text{cm}^{-1}$ . The IR spectrum positioned the peaks at 665, 862, 998, 1420 and 3570  $\text{cm}^{-1}$ . The sharp peak observed at 665 and 862  $\text{cm}^{-1}$  is ascribed to the Zn–O stretching bonds and C–O vibrations, respectively [40]. The band peak around 998  $\text{cm}^{-1}$  attributes OH bending and C–OH stretching vibrations and illustrated the existence of hydroxyl groups. This information confirmed the presence of Copper and Zinc nanophase in the prepared samples [41]. A large absorption peak at around 1420  $\text{cm}^{-1}$ , can be attributed to the  $\text{CO}_2$  presence which may be due to adsorption of air on the material surface. No obvious peaks were detected from 1500–3500  $\text{cm}^{-1}$  that indicates the complete removal of organic species and carbonates of metal precursor and conversion to oxides at high sintering temperature. The peak shown at around 3570  $\text{cm}^{-1}$  may be attributed to Cu–O–Zn bonding [42]. In addition, no sharp O–H band was obtained in 3000–3600  $\text{cm}^{-1}$  which indicates that water molecules have been eliminated in the prepared material. Conductivities measurements have been carried out with DC four probe method in air atmosphere in temperature range 300–600  $^{\circ}\text{C}$ . The corresponding results for the prepared samples are displayed in Figure 5. It can be noticed that electrical conductivities increased gradually with increase in temperature that depicts the nonmetallic behavior of material [43]. The maximum conductivity of LCZ-pure was measured to be 2.8 S/cm at 600  $^{\circ}\text{C}$ . The 1 wt.% and 1.5 wt.% graphene was incorporated in the LCZ material, and the measured results of the conductivities indicated a significant increase in conductivity values was observed from 2.8 to 3.11 and 3.5 S/cm for 1% and 1.5% incorporation of graphene in LCZ-pure, respectively. Additionally, the conductivity of material remained stable in temperature range 450–600  $^{\circ}\text{C}$ . This enhanced conductivity is attributed to development of the whitish loops over the LCZ-pure phase due to the incorporation of graphene contents. As the higher conductivity has been received in LCZ-graphene material instead of LCZ-pure material. It can be argued that this enhancement in conductivity is due to graphene incorporation. Additionally, the whitish loops in SEM images differentiate the pure and graphene incorporated material. This enhanced conductivity is attributed to development of the whitish loops over the LCZ-pure phase due to the incorporation of graphene contents. This is an evidence of graphene contents in the material. Because the obtained SEM images of LCZ-pure and LCZ-graphene incorporated indicate that the small whiteness loops and only be observed in LCZ-graphene incorporated images and not in LCZ-pure image. Therefore, it is clear that these whitish loops only represent the graphene incorporation not any other composite. Memon et al. reported that graphene may improve the electronic conductivities by loading a sufficient amount of metals or composites exhibiting higher values of electrical conductance, e.g., by employing CNT and graphene electrical conductance can be remarkably enhanced. In this regard, we have tried to incorporate graphene to improve the electrical conductivities of the material at low temperature. Further, the enhancement in electrical conductivity was observed from 10.6 S/cm to 78.7 S/cm incorporating graphene in  $\text{La}_{0.6}\text{Sr}_{0.4}\text{Al}_{0.2}\text{Cu}_{0.8}\text{O}_3$ -graphene [44].

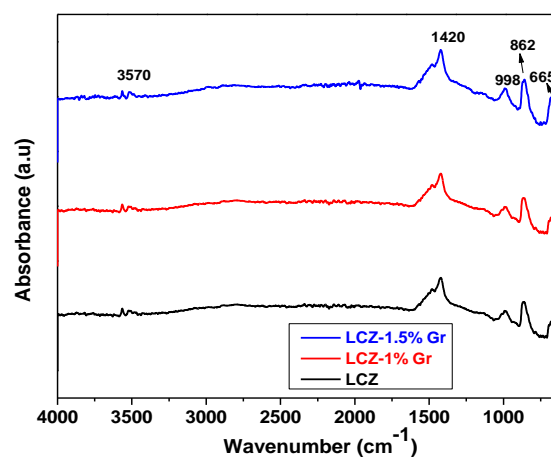


Figure 4. FTIR spectrum of prepared materials.

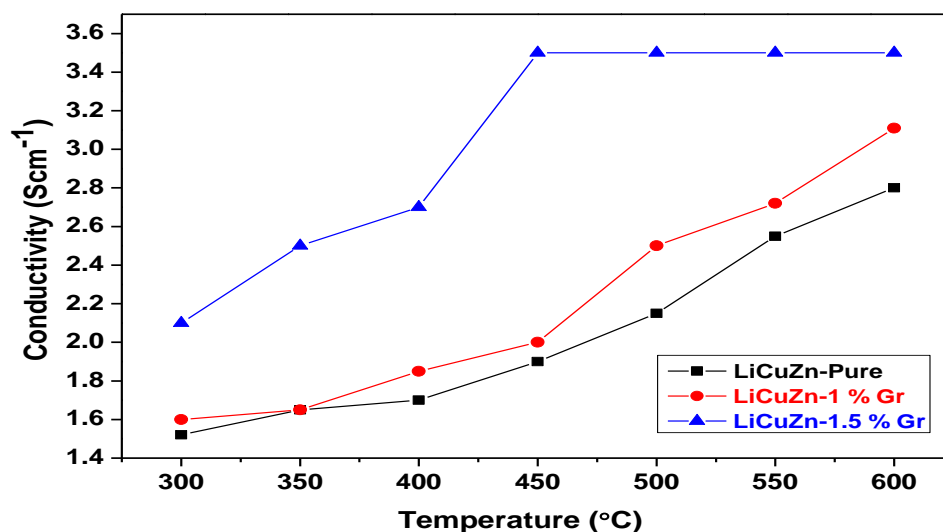


Figure 5. DC conductivity for pure LCZ and graphene incorporated nanocomposite.

The overlapping thus provided more pathways for the diffusion of gas and electrons movements through the material, and resulted in improving the conductivity. The maximum calculated values of conductivities and crystalline size are tabulated in Table 1. The electrode material exhibiting electronic conductivity greater than 1 S/cm is considered suitable for good performance of fuel cell [45]. This suggested the promising conductive behavior of graphene for electrode composite for LT-SOFC.

Table 1. Crystallite size, conductivity, and area-specific resistance (ASR) of prepared cathode samples.

Sample Name	Material Composition	Average Crystal Size (nm)	Conductivity (Scm <sup>-1</sup> ) at 600 °C	Area-specific Resistance (Ωcm <sup>2</sup> ) at 600 °C
LCZ-Pure	Li <sub>0.10</sub> Cu <sub>0.20</sub> Zn <sub>0.70</sub> -Pure	110	2.8	0.071
1 wt.% Gr-LCZ	Li <sub>0.10</sub> Cu <sub>0.20</sub> Zn <sub>0.70</sub> -1 wt.% Graphene	97	3.11	0.064
1.5 wt.% Gr-LCZ	Li <sub>0.10</sub> Cu <sub>0.20</sub> Zn <sub>0.70</sub> -1.5 wt.% Graphene	82	3.5	0.057

The area-specific resistance (ASR) of the prepared temperature dependent (300–600 °C) cathodes is illustrated in Figure 6. The minimum ASR values are determined to be 0.071, 0.064 and 0.057 Ωcm<sup>2</sup> at 600 °C for LCZ, LCZ-1 wt.%Gr, and LCZ-1.5 wt.%Gr, respectively. A relatively low ASR value (0.057 Ωcm<sup>2</sup>) is seen for LCZ-1.5% Gr sample. This minimum value of ASR suggests it to be a good cathode. The data of DC conductivity was used to plot Arrhenius curves between ln(σT) and 1/T. A linear relation was found by linear fit data as shown in Figure 7. The values of activation energies were calculated from the formula given below:

$$\sigma = \frac{A}{T} \exp\left(\frac{-E_a}{KT}\right) \quad (1)$$

where  $\sigma$  and  $E_a$  represent electrical conductivity and activation energy, while  $T$ ,  $A$ , and  $K$  are the temperature, exponential factor, and Boltzmann's constant, respectively.

The activation energies were calculated as 0.159, 0.148 and 0.139 eV. Smaller value of activation energy was found for 1.5 wt.% Gr-LCZ sample. This smaller value of activation energy demonstrated the quick chemical reaction start up for fuel cell catalytic activity [46].

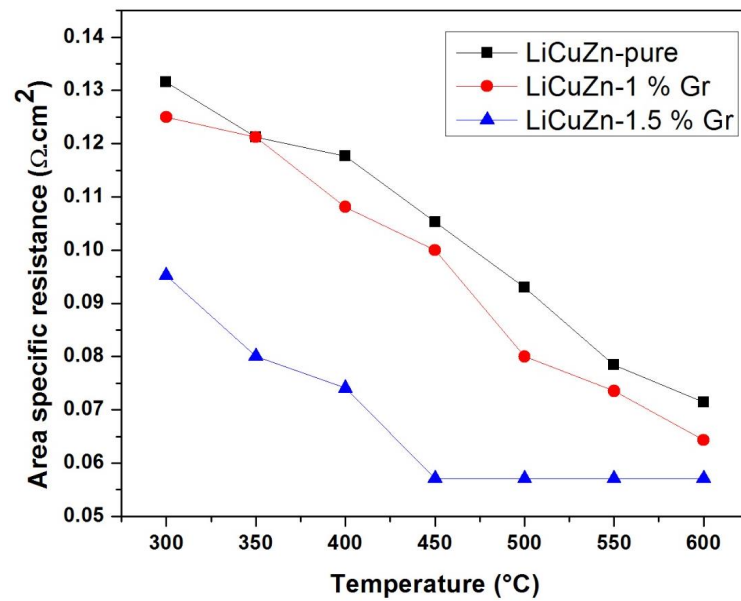


Figure 6. Area-specific resistance (ASR) of prepared cathode.

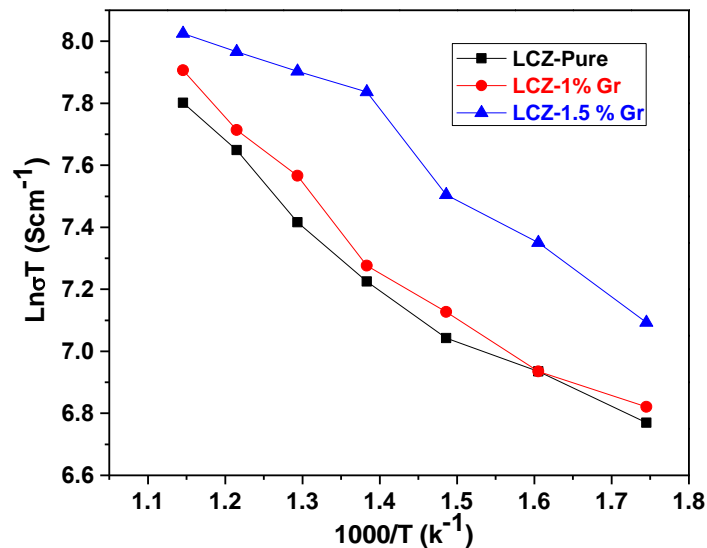


Figure 7. Arrhenius plots: (a); LCZ-pure; (b) LCZ-1 wt.% Gr (c); LCZ-1.5 wt.% Gr.

The fuel cell performance was carried out using conventional LNCZ as anode with the prepared cathode supported by NSDC dense electrolyte. The SDC, GDC, or even CDC are widely used as electrolytes for intermediate-temperature SOFC and perform good results. The carbonated coated sodium-like carbonated samarium doped ceria (NSDC) further enhance the ionic conduction at low temperature because the optical carbonated contents construct larger interface area to facilitate the proton migration [47]. Zhang 2018 also reported the powder X-ray diffraction patterns of all NSDC nanocomposites, the pattern of the controlled sample, SDC, is also included. Na<sub>2</sub>CO<sub>3</sub> crystallites are less developed than the fluorite ceria phase, almost display as the amorphous phase, since no diffraction peaks could be indexed to crystallized Na<sub>2</sub>CO<sub>3</sub> [48]. A performance test was executed with hydrogen as fuel and air as oxidant at 580 °C. The following chemical reaction occurred at the electrodes.

Oxidation at anode side:



Reduction at cathode side:



Net chemical reactions:



The open circuit voltage (OCV) values obtained from LCZ, 1 wt.% Gr-LCZ, and 1.5 wt.% Gr are 0.9, 0.9, and 0.95 V, respectively. The literature indicates that the theoretical value is 0.98 V at 600 °C, in this way, the obtained values are very close to reported theoretical value [49,50]. The maximum for each sample were found to be 225, 237 and 267 mW/cm<sup>2</sup> corresponding to obtained OCV values. Few residual pores possible to be generated due to gas cross over in electrolyte result in low value of OCV. The low OCV is obtained due to not proper dispersive of hydrogen at anode side. It also degraded due to electronic leakage. The I-V and I-P curves drawn from the collected data are shown in Figure 8. It was observed that the sample containing 1.5wt.% graphene contents yielded 18.9% enhanced power density as compared to pure LCZ cathode. The linear ohmic polarization occurred in the process reveals good electrocatalytic activity of gas reaction at cathode. The electrochemical activity took place at the triple phase boundary (TPB). The less electrochemical active area at TPB even at high temperatures may affect the migration of oxygen gases and electronic conduction. Introduction of nanoparticles catalyst increased the triple phase boundary length leading to enhance electrochemical active area at low temperature. This resulted in sufficient absorption of O<sup>2-</sup> ions and migration of electrons, which improves fuel cell performance [3]. The data of maximum value of OCV, current density, and power density determined for the developed fuel cells are listed in Table 2. The obtained power density is better than the already reported ZnO, Li<sub>2</sub>O composite which yielded maximum power density 3.86 mWcm<sup>-2</sup> at low temperatures and is comparable to the previous SOFC [51]. Further, the current results are competitive and better as compared to those reported by Xu et al. [52] for LSCFN electrode with YSZ electrolyte, recording power density 124 mW/cm<sup>2</sup> at 850 °C. This indicates the synergistic effects of graphene particles for the electrochemical application for low-temperature SOFC [53] and can readily be applied to other electrode materials as well.

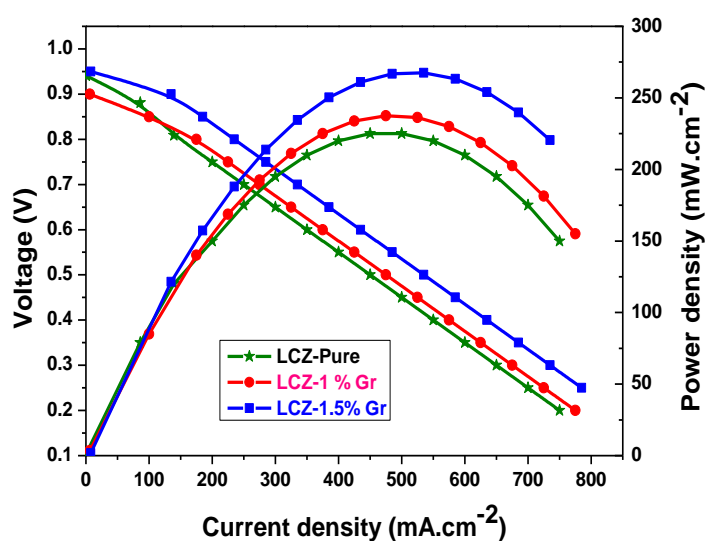


Figure 8. Fuel cell performance of prepared composite materials at 600 °C.

**Table 2.** Fuel cell performance observations at 600 °C.

Sample Name	Material Composition	Maximum OCV(V)	Current Density (mAcm <sup>-2</sup> )	Peak Power Density (mWcm <sup>-2</sup> )	References
BCZYO	BaCe <sub>0.6</sub> Zr <sub>0.2</sub> Y <sub>0.2</sub> O <sub>3-δ</sub>	0.83	1505	3.86	42
LSCFN	La <sub>0.4</sub> Sr <sub>0.6</sub> Co <sub>0.2</sub> Fe <sub>0.7</sub> Nb <sub>0.1</sub> O <sub>3-δ</sub>	1.1	900	124	43
LCZ-Pure	Li <sub>0.10</sub> Cu <sub>0.20</sub> Zn <sub>0.70</sub> -Pure	0.9	750	225	
LCZ-1%Gr	Li <sub>0.10</sub> Cu <sub>0.20</sub> Zn <sub>0.70</sub> -1 wt.% Graphene	0.9	770	237.5	Our Work
LCZ-1.5% Gr	Li <sub>0.10</sub> Cu <sub>0.20</sub> Zn <sub>0.70</sub> -1.5 wt.% Graphene	0.95	785	267.5	

#### 4. Conclusions

Graphene incorporated LCZ-oxide has been successfully prepared by a facile solid-state method as a cathode material for LT-SOFC. It is remarkable to mention that 1.5 wt.% Gr-LCZ exhibited an excellent electrical conductivity (3.5 S/cm at the rate of 450 °C). The enhanced fuel cell performance at low temperatures can be attributed to the synergistic effects contributed by the improved conductivity and low area-specific resistance that provide an efficient path for charge transport. The cell based on the same functional composition (1.5 wt.% Gr-LCZ) yielded a very good power density (267 mW/cm<sup>2</sup> at 580 °C). The obtained results provide valuable insights into the fabrication of fuel cell device based on graphene incorporated composite cathode materials for highly efficient low temperature SOFC applications.

**Author Contributions:** Conceptualization, H.L. and G.A.; methodology, M.A.A.; investigation, K.A.; data curation, A.G. and R.R.; writing—original draft preparation, M.A.A. and K.A.; writing—review and editing, M.S. and S.H.M.J.; supervision, G.A.; project administration, H.L.; and funding acquisition, H.L. All authors have read and agreed to the published version of the manuscript.

**Funding:** This research was funded by Shandong Provincial Natural Science Foundation for Excellent Young Scientists Fund Program (Overseas) (Grant No.: 2022HWYQ-060), Shandong Provincial Natural Science Foundation (Grant No.: ZR2021QE148), Guangdong Basic and Applied Basic Research Foundation (Grant No.: 2022A1515011473). The authors extend their appreciation to the Deanship of Scientific Research at King Khalid University for funding this work through Research Groups Program under grant number (RGP.1/196/43).

**Data Availability Statement:** All relevant data are presented in the manuscript. Any other details about data or raw data are available upon request from the corresponding author.

**Conflicts of Interest:** The authors declare no conflict of interest.

#### References

- Winter, U.; Weidner, H. Hydrogen for the mobility of the future results of GM/Opel's well-to-wheel studies in north America and Europe. *Fuel Cells* **2003**, *3*, 76–83. [CrossRef]
- Abdalla, A.M.; Hossain, S.; Azad, A.T.; Petra, P.M.I.; Begum, F.; Eriksson, S.G.; Azad, A.K. Nanomaterials for solid oxide fuel cells: A review. *Renew. Sustain. Energy Rev.* **2018**, *82*, 353–368. [CrossRef]
- Abbas, G.; Raza, R.; Ashfaq, M.; Chaudhry, M.; Khan, A.; Ahmad, I.; Zhu, B. Electrochemical study of nanostructured electrode for low-temperature solid oxide fuel cell (LT-SOFC). *Int. J. Energy Res.* **2014**, *38*, 518–523. [CrossRef]
- Solid Oxide Fuel Cells, Illinois Institute of Technology Notes. Available online: <https://mypages.iit.edu/~smart/garrear/fuelcells.htm> (accessed on 5 February 2018).
- Mumtaz, S.; Ahmad, M.A.; Raza, R.; Arshad, M.S.; Ahmed, B.; Ashiq, M.N.; Abbas, G. Nano grained Sr and Zr co-doped BaCeO<sub>3</sub> electrolytes for intermediate temperature solid oxide fuel cells. *Ceram. Int.* **2017**, *43*, 14354–14360. [CrossRef]
- Liu, F.; Diercks, D.; Hussain, A.M.; Dale, N.; Furuya, Y.; Miura, Y.; Fukuyama, Y.; Duan, C. Nanocomposite Catalyst for High-Performance and Durable Intermediate-Temperature Methane-Fueled Metal-Supported Solid Oxide Fuel Cells. *ACS Appl. Mater. Interfaces* **2022**, *14*, 53840–53849. [CrossRef]
- Liu, F.; Duan, C. Direct-Hydrocarbon Proton-Conducting Solid Oxide Fuel Cells. *Sustainability* **2021**, *13*, 4736. [CrossRef]
- Suda, S.; Itagaki, M.; Node, E.; Takahashi, S.; Kawano, M.; Yoshida, H.; Inagaki, T. Preparation of SOFC anode composites by spray pyrolysis. *J. Eur. Ceram. Soc.* **2006**, *26*, 593–597. [CrossRef]
- Khan, M.A.; Xu, C.; Song, Z.; Raza, R.; Ahmad, M.A.; Abbas, G.; Zhu, B. Synthesize and characterization of ceria based nano-composite materials for low temperature solid oxide fuel cell. *Int. J. Hydrog. Energy* **2018**, *43*, 6310–6317. [CrossRef]

10. Fang, X.; Zhu, G.; Xia, C.; Liu, X.; Meng, G. Synthesis and properties of Ni-SDC cermet for IT-SOFC anode by co-precipitation. *Solid State Ion.* **2004**, *168*, 31–36. [[CrossRef](#)]
11. Yang, C.; Yang, Z.; Jin, C.; Xiao, G.; Chen, F.F.; Han, M. Sulfur-Tolerant redox-reversible anode material for direct hydrocarbon solid oxide fuel cells. *Adv. Mater.* **2012**, *24*, 1439–1443. [[CrossRef](#)]
12. Misono, T.; Murata, K.; Fukui, T.; Chaichanawong, J.; Sato, K.; Abe, H.; Naito, M. Ni-SDC cermet anode fabricated from NiO-SDC composite powder for intermediate temperature SOFC. *J. Power Sources* **2006**, *157*, 754–757. [[CrossRef](#)]
13. Wang, W.G.; Mogensen, M.B. High-performance lanthanum-ferrite-based cathode for SOFC. *Solid State Ion.* **2005**, *176*, 457–462. [[CrossRef](#)]
14. Tietz, F.; Buchkremer, H.-P.; Stöver, D. Components manufacturing for solid oxide fuel cells. *Solid State Ion.* **2002**, *152*, 249–259. [[CrossRef](#)]
15. Huang, K.; Lee, H.; Goodenough, J. Sr and Ni-doped LaCoO<sub>3</sub> and LaFeO<sub>3</sub> perovskites new cathode materials for solid-oxide fuel cells. *J. Electrochem. Soc.* **1998**, *145*, 3220–3227. [[CrossRef](#)]
16. Jun, A.; Yoo, S.; Gwon, O.; Shin, J.; Kim, G. Thermodynamic and electrical properties of Ba<sub>0.5</sub>Sr<sub>0.5</sub>Co<sub>0.8</sub>Fe<sub>0.2</sub>O<sub>3-δ</sub> and La<sub>0.6</sub>Sr<sub>0.4</sub>Co<sub>0.2</sub>Fe<sub>0.8</sub>O<sub>3-δ</sub> for intermediate-temperature solid oxide fuel cells. *Electrochim. Acta* **2013**, *89*, 372–376. [[CrossRef](#)]
17. Ahmad, K.; Abbas, G.; Ahmad, M.A. Structural and electrical study of nanocomposite Fe<sub>0.2</sub>Ni<sub>0.3</sub>Cu<sub>0.5</sub> anode with effect of graphene oxide (GO) for low-temperature SOFCs. *Int. J. Energy Res.* **2022**, *46*, 16949–16958. [[CrossRef](#)]
18. Zhu, B.; Liu, X.; Zhou, P.; Yang, X.; Zhu, Z.; Zhu, W. Innovative solid carbonate-ceria composite electrolyte fuel cells. *Fuel Cells Bull.* **2001**, *2002*, 8–12. [[CrossRef](#)]
19. Raza, R.; Wang, X.; Ma, Y.; Zhu, B. A nanostructure anode (Cu<sub>0.2</sub>Zn<sub>0.8</sub>) for low-temperature solid oxide fuel cell at 400–600 °C. *J. Power Sources* **2010**, *195*, 8067–8070. [[CrossRef](#)]
20. Zhu, B.; Raza, R.; Abbas, G.; Singh, M. An electrolyte-free fuel cell constructed from one homogenous layer with mixed conductivity. *Adv. Funct. Mater.* **2011**, *21*, 2465–2469. [[CrossRef](#)]
21. Raza, R.; Abbas, G.; Liu, Q.; Pate, I.; Zhu, B. La<sub>0.3</sub>Sr<sub>0.2</sub>Mn<sub>0.1</sub>Zn<sub>0.4</sub> Oxide-Sm<sub>0.2</sub>Ce<sub>0.8</sub>O<sub>1.9</sub> (LSMZ-SDC) Nanocomposite Cathode for Low Temperature SOFCs. *J. Nanosci. Nanotechnol.* **2012**, *12*, 4994–4997. [[CrossRef](#)]
22. Fan, L.; Zhu, B.; Chen, M.; Wang, C.; Raza, R.; Qin, H.; Wang, X.; Wang, X.; Ma, Y. High performance transition metal oxide composite cathode for low temperature solid oxide fuel cells. *J. Power Sources* **2012**, *203*, 65–71. [[CrossRef](#)]
23. Hussain, M.; Raza, R.; Ahmad, M.; Ali, A.; Ahmad, I.; Syed, W.; Abbas, G. Electrochemical study of natural gas fueled electrodes for low temperature solid oxide fuel cell. *Int. J. Mod. Phys. B* **2016**, *30*, 1650161. [[CrossRef](#)]
24. Allen, M.J.; Tung, V.C.; Kaner, R.B. Honeycomb Carbon: A Review of Graphene. *Chem. Rev.* **2009**, *110*, 132–145. [[CrossRef](#)] [[PubMed](#)]
25. Jee, Y.; Karimghaloo, A.; Andrade, A.M.; Moon, H.; Li, Y.; Han, J.; Ji, S.; Ishihara, H.; Su, P.; Cha, S.W.; et al. Graphene-based Oxygen Reduction Electrodes for Low Temperature Solid Oxide Fuel Cells. *Fuel Cells* **2017**, *17*, 344–352. [[CrossRef](#)]
26. Marinha, D.; Belmonte, M. Mixed-ionic and electronic conduction and stability of YSZ-graphene composites. *J. Eur. Ceram. Soc.* **2019**, *39*, 389–395. [[CrossRef](#)]
27. Zheng, B.; Wang, J.; Wang, F.-B.; Xia, X.-H. Low-loading cobalt coupled with nitrogen-doped porous graphene as excellent electrocatalyst for oxygen reduction reaction. *J. Mater. Chem. A* **2014**, *2*, 9079–9084. [[CrossRef](#)]
28. Fuchsichler, B.; Stangl, C.; Kren, H.; Uhlig, F.; Koller, S. High capacity graphite-silicon composite anode material for lithium-ion batteries. *J. Power Sources* **2011**, *196*, 2889–2892. [[CrossRef](#)]
29. Wu, Z.-S.; Ren, W.; Wen, L.; Gao, L.; Zhao, J.; Chen, Z.; Zhou, G.; Li, F.; Cheng, H.-M. Graphene Anchored with Co<sub>3</sub>O<sub>4</sub> Nanoparticles as Anode of Lithium Ion Batteries with Enhanced Reversible Capacity and Cyclic Performance. *ACS Nano* **2010**, *4*, 3187–3194. [[CrossRef](#)]
30. Pollak, E.; Geng, B.; Jeon, K.; Lucas, I.; Richardson, T.; Wang, F.; Kosteki, R. The interaction of Li<sup>+</sup> with single-layer and few-layer graphene. *Nano Lett.* **2010**, *10*, 3386–3388. [[CrossRef](#)]
31. Aslam, S.; Mustafa, F.; Ahmad, M. Facile synthesis of graphene oxide with significant enhanced properties for optoelectronic and energy devices. *Ceram. Int.* **2018**, *44*, 6823–6828. [[CrossRef](#)]
32. Zhao, Y.; He, J.; Fan, L.; Ran, W.; Zhang, C.; Gao, D.; Gao, F. Synthesis and characterization of hierarchical porous LiNi-CuZn-oxides as potential electrode materials for low temperature solid oxide fuel cells. *Int. J. Hydrog. Energy* **2013**, *38*, 16558–16562. [[CrossRef](#)]
33. Zhang, L.; Xiao, J.; Xie, Y.; Tang, Y.; Liu, J.; Liu, M. Behavior of strontium- and magnesium-doped gallate electrolyte in direct carbon solid oxide fuel cells. *J. Alloys Compd.* **2014**, *608*, 272–277. [[CrossRef](#)]
34. Zhang, L.; Lan, R.; Kraft, A.; Tao, S. A stable intermediate temperature fuel cell based on doped-ceria-carbonate composite electrolyte and perovskite cathode. *Electrochem. Commun.* **2011**, *13*, 582–585. [[CrossRef](#)]
35. Li, S.; Lü, Z.; Huang, X.; Wei, B.; Su, W. Electrical and thermal properties of (Ba<sub>0.5</sub>Sr<sub>0.5</sub>)<sub>1-x</sub>SmxCo<sub>0.8</sub>Fe<sub>0.2</sub>O<sub>3-δ</sub> perovskite oxides. *Solid State Ion.* **2007**, *178*, 417–422. [[CrossRef](#)]
36. Cai, D.; Song, M. Preparation of fully exfoliated graphite oxide nanoplatelets in organic solvents. *J. Mater. Chem.* **2007**, *17*, 3678–3680. [[CrossRef](#)]
37. Yang, Z.; Xu, N.; Han, M.; Chen, F. Performance evaluation of La<sub>0.4</sub>Sr<sub>0.6</sub>Co<sub>0.2</sub>Fe<sub>0.7</sub>Nb<sub>0.1</sub>O<sub>3-δ</sub> as both anode and cathode material in solid oxide fuel cells. *Int. J. Hydrog. Energy* **2014**, *39*, 7402–7406. [[CrossRef](#)]

38. Du, Z.; Zhao, H.; Yi, S.; Xia, Q.; Gong, Y.; Zhang, Y.; Świerczek, K. High-performance anode material  $\text{Sr}_2\text{FeMo}_{0.65}\text{Ni}_{0.35}\text{O}_{6-\delta}$  with in situ exsolved nanoparticle catalyst. *ACS Nano* **2016**, *10*, 8660–8669. [[CrossRef](#)]
39. Esmaeili, Y.; Bidram, E.; Zarrabi, A.; Amini, A.; Cheng, C. Graphene oxide and its derivatives as promising In-vitro bio-imaging platforms. *Sci. Rep.* **2020**, *10*, 18052. [[CrossRef](#)]
40. Xiong, H.; Shchukin, D.; Möhwald, H.; Xu, Y.; Xia, Y. Sonochemical synthesis of highly luminescent zinc oxide nano-particles doped with magnesium (II). *Angew Chem. Int. Ed.* **2009**, *48*, 2727–2731. [[CrossRef](#)]
41. Umar, A.; Lee, J.-H.; Kumar, R.; Al-Dossary, O.; Ibrahim, A.A.; Baskoutas, S. Development of highly sensitive and selective ethanol sensor based on lance-shaped CuO nanostructures. *Mater. Des.* **2016**, *105*, 16–24. [[CrossRef](#)]
42. Korkishko, Y.; Fedorov, V. *Ion Exchange in Single Crystals for Integrated Optics and Optoelectronics*; Cambridge Int Science Publishing: Great Abington, UK, 1999.
43. Fan, L.; Wang, C.; Osamudiamen, O.; Raza, R.; Singh, M.; Zhu, B. Mixed ion and electron conductive composites for single component fuel cells: I. Effects of composition and pellet thickness. *J. Power Sources* **2012**, *217*, 164–169. [[CrossRef](#)]
44. Memon, S.A.; Shaikh, H.I.; Raza, R.; Mughal, Z.U.N.; Memon, A.A.; Memon, S. Graphene incorporated mesoporous perovskite with excellent conductivity and catalytic activity for low temperature solid oxide fuel cells. *New J. Chem.* **2022**, *46*, 12530–12539. [[CrossRef](#)]
45. McIntosh, S.; Gorte, R.J. Direct Hydrocarbon Solid Oxide Fuel Cells. *Chem. Rev.* **2004**, *104*, 4845–4866. [[CrossRef](#)] [[PubMed](#)]
46. Kong, W.; Zhang, M.; Han, Z.; Zhang, Q. A Theoretical Model for the Triple Phase Boundary of Solid Oxide Fuel Cell Electrospun Electrodes. *Appl. Sci.* **2019**, *9*, 493. [[CrossRef](#)]
47. Wang, X.; Ma, Y.; Raza, R.; Muhammed, M.; Zhu, B. Novel core-shell SDC/amorphous  $\text{Na}_2\text{CO}_3$  nanocomposite electrolyte for low-temperature SOFCs. *Electrochem. Commun.* **2008**, *10*, 1617–1620. [[CrossRef](#)]
48. Zhang, G.; Li, W.; Huang, W.; Cao, Z.; Shao, K.; Li, F.; Tang, C.; Li, C.; Chuanxin, H.; Zhang, Q.; et al. Strongly coupled  $\text{Sm}_{0.2}\text{Ce}_{0.8}\text{O}_2$ - $\text{Na}_2\text{CO}_3$  nanocomposite for low temperature solid oxide fuel cells: One-step synthesis and super interfacial proton conduction. *J. Power Sources* **2018**, *386*, 56–65. [[CrossRef](#)]
49. Solovyev, A.; Shipilova, A.; Smolyanskiy, E.; Rabotkin, S.; Semenov, V. The properties of intermediate-temperature solid oxide fuel cells with thin film gadolinium-doped ceria electrolyte. *Membranes* **2022**, *12*, 896. [[CrossRef](#)]
50. Matsui, T.; Kosaka, T.; Inaba, M.; Mineshige, A.; Ogumi, Z. Effects of mixed conduction on the open-circuit voltage of intermediate temperature SOFCs based on Sm-doped ceria electrolytes. *Solid State Ion.* **2005**, *176*, 663–668. [[CrossRef](#)]
51. Zagórski, K.; Wachowski, S.; Szymczewska, D.; Mielewczyk-Gryń, A.; Jasiński, P.; Gazda, M. Performance of a single layer fuel cell based on a mixed proton-electron conducting composite. *J. Power Sources* **2017**, *353*, 230–236. [[CrossRef](#)]
52. Xu, N.; Zhu, T.; Yang, Z.; Han, M. Fabrication and optimization of  $\text{La}_{0.4}\text{Sr}_{0.6}\text{Co}_{0.2}\text{Fe}_{0.7}\text{Nb}_{0.1}\text{O}_{3-\delta}$  electrode for symmetric solid oxide fuel cell with zirconia based electrolyte. *J. Mater. Sci. Technol.* **2017**, *33*, 1329–1333. [[CrossRef](#)]
53. Tan, C.; Huang, X.; Zhang, H. Synthesis and applications of graphene-based noble metal nanostructures. *Mater. Today* **2013**, *16*, 29–36. [[CrossRef](#)]

**Disclaimer/Publisher's Note:** The statements, opinions and data contained in all publications are solely those of the individual author(s) and contributor(s) and not of MDPI and/or the editor(s). MDPI and/or the editor(s) disclaim responsibility for any injury to people or property resulting from any ideas, methods, instructions or products referred to in the content.